Bioactive Materials 6 (2021) 1189–1200

Contents lists available at ScienceDirect

Bioactive Materials

journal homepage: www.sciencedirect.com/journal/bioactive-materials

# Construction of tantalum/poly(ether imide) coatings on magnesium implants with both corrosion protection and osseointegration properties

Kwang-Hee Cheon [a], Cheonil Park [a], Min-Ho Kang [a], In-Gu Kang [a], Min-Kyu Lee [a], Hyun Lee [c], Hyoun-Ee Kim [a], Hyun-Do Jung [b,*], Tae-Sik Jang [d,**]

[a] Department of Materials Science and Engineering, Seoul National University, Seoul, Republic of Korea
[b] Department of Biomedical-Chemical Engineering, Catholic University of Korea, Bucheon, Gyeonggi-do, Republic of Korea
[c] Institute of Health Science Research, Korea University, Seoul, 02841, Republic of Korea
[d] Department of Materials Science and Engineering, Chosun University, Gwangju, Republic of Korea

ARTICLE INFO

*Keywords:*
Magnesium
Tantalum
Poly(ether imide)
Bio-functionalized coating
Biodegradable orthopedic implants

ABSTRACT

Poly(ether imide) (PEI) has shown satisfactory corrosion protection capability with good adhesion strength as a coating for magnesium (Mg), a potential candidate of biodegradable orthopedic implant material. However, its innate hydrophobic property causes insufficient osteoblast affinity and a lack of osseointegration. Herein, we modify the physical and chemical properties of a PEI-coated Mg implant. A plasma immersion ion implantation technique is combined with direct current (DC) magnetron sputtering to introduce biologically compatible tantalum (Ta) onto the surface of the PEI coating. The PEI-coating layer is not damaged during this process owing to the extremely short processing time (30 s), retaining its high corrosion protection property and adhesion stability. The Ta-implanted layer (roughly 10-nm-thick) on the topmost PEI surface generates long-term surface hydrophilicity and favorable surface conditions for pre-osteoblasts to adhere, proliferate, and differentiate. Furthermore, in a rabbit femur study, the Ta/PEI-coated Mg implant demonstrates significantly enhanced bone tissue affinity and osseointegration capability. These results indicate that Ta/PEI-coated Mg is promising for achieving early mechanical fixation and long-term success in biodegradable orthopedic implant applications.

## 1. Introduction

Magnesium (Mg) and its alloys have attracted significant attention as promising orthopedic implant materials owing to their biodegradable abilities and suitable mechanical properties [1–4]. As Mg has an elastic modulus similar to human bone, it can minimize the stress shielding effect while providing adequate mechanical support for physiological loads at fracture sites [1,3,5]. In addition, as Mg ions have osteogenic and osteopromotive effects, the degradation behavior of Mg implants provides a beneficial stimulus (and thus favorable treatment) for patients with osteoporosis or osteopenia [6–9]. However, despite these advantageous in bone remodeling and repair, Mg has an excessively high corrosion rate in physiological conditions, which is a major obstacle for practical applications [10–14].

To solve critical limitations of practical applications, considerable research has been actively conducted to improve the corrosion resistance of Mg, including alloying with other metallic elements or fabricating bioceramic or polymeric coating layers on the surface of Mg [15,16]. Among these methods, polymeric coating systems can reduce the corrosion rate of Mg by providing a physical barrier, thereby preventing direct contact between Mg and any surrounding corrosive medium [17–19]. Moreover, polymers have versatile physical and chemical properties that offer various options for corrosion protection [20,21]. Over the past few decades, many synthetic polymers, such as poly(lactic acid), poly(L-lactic-co-glycolic acid), poly(dioxanone), poly(1, 3-trimethylene carbonate), and poly(ether imide) (PEI), have been developed to explore their feasibility as protective implant coatings [6, 22–24]. These polymers have well-ordered long hydrophobic chains, which are functionally related to reducing aqueous solution penetration toward the surface of Mg substrates, thereby withstanding corrosive attacks [19]. However, these hydrophobic surface characteristics also reduce the accessible environment to cell-containing media, resulting in poor osteoblast affinity and thus a lack of direct bone-to-implant contact, which is commonly referred to as osseointegration [25].

* Corresponding author.
** Corresponding author.
*E-mail addresses:* hdjung@catholic.ac.kr (H.-D. Jung), tsjang@chosun.ac.kr (T.-S. Jang).

https://doi.org/10.1016/j.bioactmat.2020.10.007
Received 1 July 2020; Received in revised form 12 October 2020; Accepted 14 October 2020

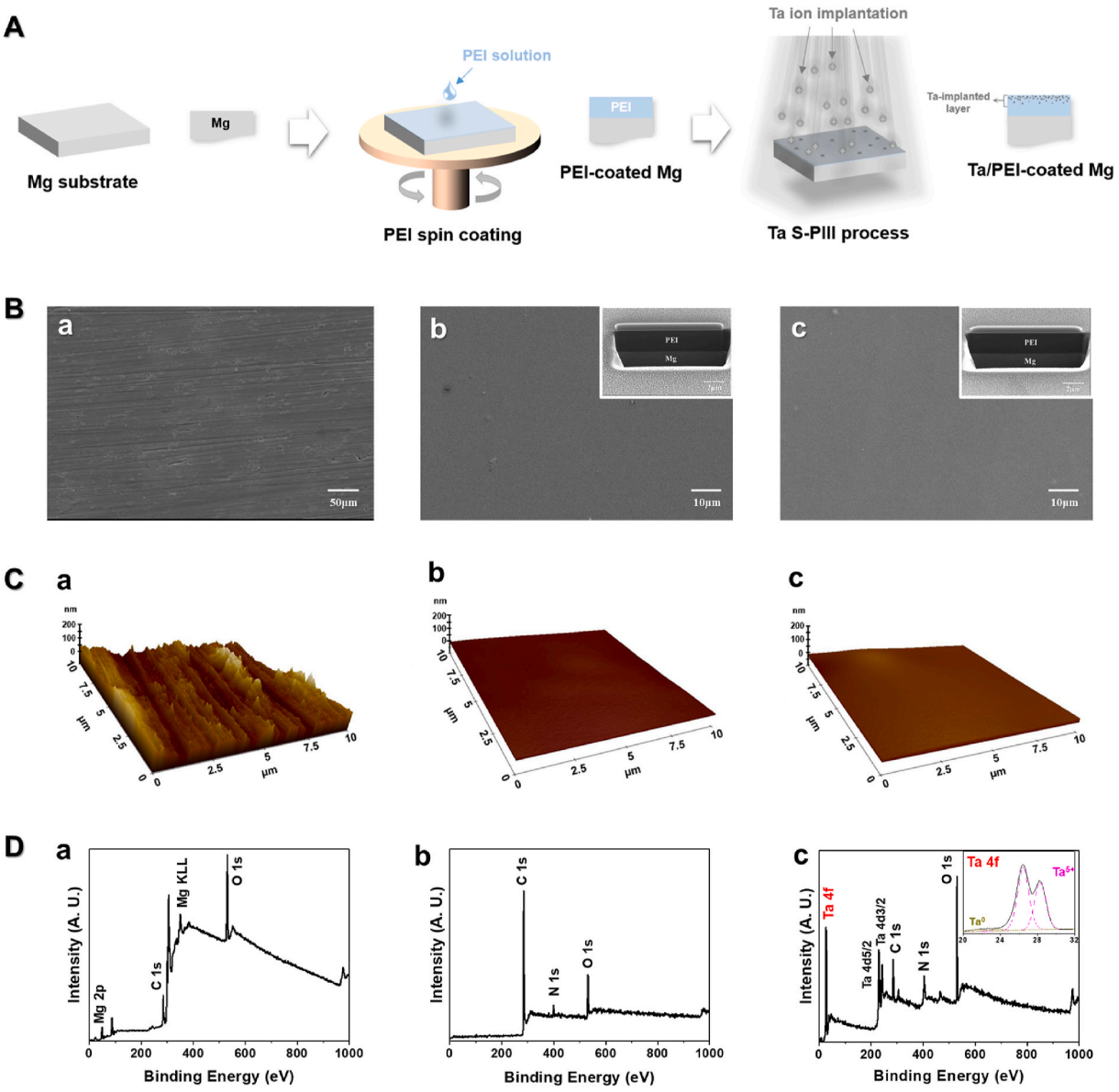


**Fig. 1.** (A) Schematic of sequential PEI coating and Ta S-PIII surface treatment on the bare Mg substrate. (B) Surface morphologies and (C) AFM topographical 3D maps of the (a) bare, (b) PEI-coated, and (c) Ta/PEI-coated Mg samples. Insets in B show cross-sectional SEM images of the surface coatings. (D) XPS full spectra obtained from the surface of (a) bare, (b) PEI-coated, and (c) Ta/PEI-coated Mg samples; inset in the top-right-hand corner of (c) is the high-resolution spectrum of Ta 4f.

Recent advances in plasma immersion ion implantation (PIII) techniques have provided promising opportunities to solve this problematic relationship. The unique capability of PIII to alter the polymer surface in a relatively active state via ionizing radiation is beneficial with respect to ameliorating surface hydrophobicity without negatively affecting corrosion protection properties [26,27]. In this technique, ions in plasma are accelerated toward the substrate surface under applied substrate biases with excellent conformity to the substrate shape, which renders the homogenous modification of the whole surface possible regardless of sample geometry [26]. Additionally, an ion-implanted surface layer can be used to facilitate interfacial strength owing to its structural continuity within the substrate, thereby ensuring mechanical stability and reliability [27]. However, the PIII technique has only been applied to highly thermally resistant polymers because it has a long processing time. Typically, it takes several hours to modify the polymer surface, which results in substantial heat accumulation in the ion-irradiated area, which subsequently causes the thermal deformation, decomposition, and destruction of the polymer [25–27]. Therefore, to successfully modify the surface of polymer-coated Mg implants, a rapid and efficient PIII technique is required.

The recently developed sputtering-based PIII (S-PIII) technique generates numerous metallic ions from a direct current (DC) magnetron sputtering gun, which ensures massive metal ion implantation onto a polymeric substance at high doses while reducing the processing time to a few tens of seconds, thereby minimizing thermal damage of the polymeric substrate and widening the practical applications of the PIII technique [25,28,29]. In particular, because tantalum (Ta) is biocompatible and has excellent osseointegration abilities, when used as a metal ion source, it provides a favorable surface environment for the adhesion and growth of osteoblast cells, subsequently promoting new bone formation and integration between an implant and the surrounding bone tissue [25,27,30–32].

Herein, to investigate the practical feasibility and effectiveness of S-PIII, PEI is used as a representative polymeric coating material for a Mg implant owing to its outstanding corrosion protection ability and strong adhesiveness to the Mg surface; it also has a poor biological response to

the host bone [24,33–35]. Spin-coating is used to form the uniform PEI-coating layer on the Mg substrate, following which the S-PIII treatment is performed with Ta ions, creating the Ta/PEI-coated Mg; then, changes in surface characteristics, corrosion protection ability, wettability, and osteoblast responses are evaluated and compared with bare Mg.

## 2. Experimental section

**Sample preparation**. Mg alloy WE43 (yttrium (4.1 wt%), neodymium (2.1 wt%), zirconium (0.56 wt%), manganese (0.028 wt%), and balance Mg (Yueyang Yuhua Yejin company, China) was used as a model Mg substrate because it is widely used in orthopedic applications. The overall coating procedure is shown in Fig. 1A. The Mg alloy was cut into a square (10 × 10 × 2 mm), polished using abrasive silicon carbide (SiC) paper (up to 2000 grit), and cleaned and sonicated in ethanol using an ultrasonic bath. PEI pellets (Sigma–Aldrich, USA) were dissolved in N-methyl-2-pyrollidone (Sigma–Aldrich, USA) at a concentration of 15% w/v. The solution was stirred overnight at a temperature of 37 °C. The PEI solution was spin-coated on the Mg substrate at 2000 rpm for 1 min; the coated samples were then dried at 70 °C for 24 h to remove residual solvent and densify the PEI-coating layer. Post PEI coating and drying, the specimens were placed in a vacuum chamber. A Ta target with a diameter of 75 mm, thickness of 5 mm, and purity of 99.99% (Kojundo Chemical Lab, Japan) was laid in a DC magnetron sputter gun housing (Ultech Co., Ltd., Korea). After the chamber was pressurized to $5 \times 10^{-4}$ Pa using a rotary pump and diffusion pump, the S-PIII technique was used to subject the PEI-coated Mg specimens to the Ta target under a negative voltage of 2000 V for 30 s with an argon gas flow of 7 mTorr. A target current of 50 mA was applied with no additional heating [25].

**Characterization of the tantalum/poly(ether imide)-coating layer**. The surface morphologies of the bare Mg, the PEI-coated Mg, and the Ta/PEI-coated Mg were observed with field-emission scanning electron microscopy (FE-SEM; MERLIN Compact, ZEISS, Germany); the thickness of the PEI-coating layer was assessed via FE-SEM and focused ion beam (FIB). The surface roughness of the bare Mg, the PEI-coated Mg, and the Ta/PEI-coated Mg was examined via atomic force microscopy (AFM; PAFM NX, EM4SYS Co., Ltd., Korea) under the non-contact mode; the size of the characterized region was 10 × 10 μm. The surface chemistry of the PEI-coated Mg and the Ta/PEI-coated Mg was evaluated via FE-SEM coupled with energy-dispersive X-ray spectroscopy (EDS) and X-ray photoelectron spectroscopy (XPS; Axis Supra, Kratos, England). The cross-section of the Ta/PEI-coating layer was obtained via transmission electron microscopy (TEM; JEM-2100F, JEOL, Japan), and the element linear profile was analyzed through energy dispersive X-ray spectroscopy (EDS) analysis affiliated with TEM. The adhesion strength of the PEI- and Ta/PEI-coating layer on Mg substrate was measured using the pull-out method (RB302 single column type, R&B, Korea). A pre-epoxy-coated stud was placed on the surface of the samples and cured at 150 °C for 15 min by increasing the temperature at a rate of 5 °C/min. The attached stud on the coating layer was pulled away using a tensile machine (Microload system, R&B, Korea) at a speed of 1 mm/min until the coating layer was fully detached from the Mg substrate. Three samples were used for each coating condition. To measure the hydrophilicities of the bare Mg, the PEI-coated Mg, and the Ta/PEI-coated Mg, contact angles were identified using a distilled water droplet on the Phoenix 300 contact angle analyzer (Surface Electro Optics Co., Ltd., Korea) [36]. Additionally, the longevity of the modified surface under wet conditions was monitored through immersion in a phosphate-buffered saline (PBS) solution for one week. The contact angle was calculated using the ImageJ software (National Institute of Health, Bethesda, USA).

**Evaluating the corrosion behavior of the tantalum/poly(ether imide)-coated magnesium**. The corrosion behavior was confirmed by measuring the amount of generated hydrogen ($H_2$) gas and the pH variation during corrosion after the bare Mg, PEI-coated Mg, and Ta/PEI-coated Mg were immersed in simulated body fluid (SBF) at a temperature of 37 °C for 10 days. The SBF was prepared according to the method presented by Kokubo et al. [37]. Prior to immersion in SBF, the uncoated side of the Mg samples was mounted using epoxy resin. Using the amount of generated $H_2$ gas, the *in vitro* corrosion rate was calculated based on the following stoichiometry:

$$Mg + 2H_2O \rightarrow Mg(OH)_2 + H_2.$$

The pH value was monitored using a pH meter (Orion 3 Star; ThermoFisher Scientific, Waltham, MA, USA). The volume change of the Mg cylinder was monitored through micro computed tomography (μ-CT; Skyscan 1173, Konitch, Belgium) at day 0, 3, 6, and 14 under the following conditions: a resolution of 18 μm using a 1-mm aluminum filter, a voltage of 130 kV, and a current of 60 mA. Prior to the corrosion test, a Mg cylinder was prepared from the WE43 ingot with a diameter of 4 mm and a length of 6 mm. The samples were polished with 2000 SiC paper and cleaned with ethanol. Following the cleaning process in ethanol with ultrasonic bath, the PEI was coated onto the Mg cylinder with a dipping procedure at a withdrawal speed of 1 mm/min. The coating procedure was repeated twice and the Mg cylinder was dried at 70 °C overnight. The thickness of the PEI coating layer was set to match that of the spin-coated sample. Following the PEI coating, the S-PIII technique was performed under the same conditions as the substrate samples; both ends of the Mg cylinder were mounted with epoxy resin. After all samples were immersed in the SBF, the morphologies and volume of the cylinder were monitored and calculated using commercial analysis software (CTAn, Bruker, Belgium) for 14 days, and the three-dimensional (3D) structural images of the corroded samples were identified using post-processing software (CTVox, Bruker, Belgium). A set threshold was used to obtain the image that eliminated the corrosion product from the Mg alloy body.

**Evaluating *in vitro* biological performance of the tantalum/poly (ether imide)-coated magnesium**. The initial cell attachment, proliferation, and differentiation of the pre-osteoblast cells (MC3T3-E1; CRL-2593, ATCC, USA) was evaluated on the bare Mg, the PEI-coated Mg, and the Ta/PEI-coated Mg. The cells were cultured in an alpha minimum essential medium (Welgene Biotech Co., Ltd., Korea) supplemented with 10% fetal bovine serum and 1% penicillin–streptomycin in a humidified incubator with 5% carbon dioxide at 37 °C. Prior to the *in vitro* cell test, all samples were rinsed with ethanol and subsequently placed on a clean bench and sterilized with ultraviolet light for 24 h.

The initial cell attachment was confirmed using confocal laser microscopy (CLSM; LSM710, Carl Zeiss, Germany) after culturing for 6 and 24 h with a seeding density of $3 \times 10^4$ cells/mL on the bare Mg, the PEI-coated Mg, and the Ta/PEI-coated Mg. Post culturing, the samples were washed with PBS with a pH of 7.4 (Welgene Biotech Co., Ltd., Korea) and stained with a live/dead assay (L3224, Invitrogen, Carlsbad, USA) for 30 min in the dark.

The cell proliferation of the pre-osteoblast cells on the bare Mg, the PEI-coated Mg, and the Ta/PEI-coated Mg was investigated by quantifying the amount of DNA for the cells attached on the samples using a CyQUANT cell proliferation assay kit (C7026, Invitrogen, Carlsbad, USA) after culturing for 24 h and then three and five days with a density of $3 \times 10^4$ cells/mL. The culture medium was refreshed every day after the cells were seeded. Post culturing, the cells on the samples were detached using 0.25% trypsin–EDTA for 4 min at 37 °C, and the suspension containing the detached cells was treated using a fluorescent dye solution. The DNA level of the detached cells was quantified using a multiple plate reader (Victor3, PerkinElmer Inc., Germany). When performing measurements, the excitation and emission wavelengths were 495 and 520 nm, respectively.

Cell differentiation of the pre-osteoblast cells on the bare Mg, the PEI-coated Mg and the Ta/PEI-coated Mg was conducted using an alkaline phosphatase (ALP) activity assay after culturing for 10 days with a density of $0.5 \times 10^4$ cells/mL. To accelerate the cell differentiation, β-GP of 10 mM and ascorbic acid of 50 mg/mL were added to the culture medium after culturing for 24 h and the culture medium was

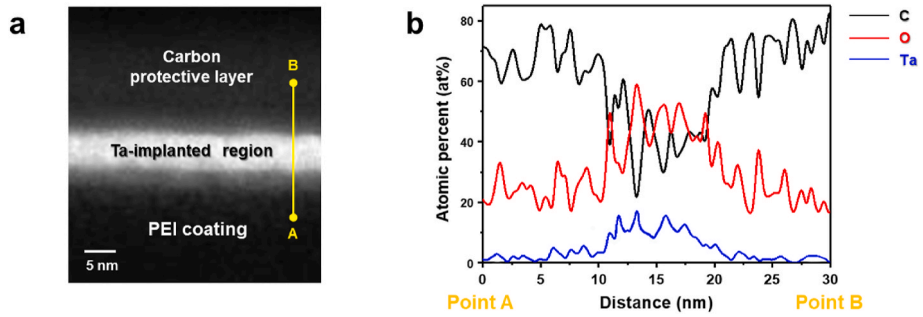


**Fig. 2.** (a) High-resolution cross-sectional STEM image of Ta/PEI-coated Mg and (b) STEM/EDS compositional profiles of C (black), O (red), and Ta (blue) through the yellow line from point A to B shown in (a).

refreshed every three days. The ALP activity was examined at a wavelength of 405 nm using a micro reader (Model 550, Bio-Rad Laboratories, USA). The number of the samples was three specimens for each condition. The number of the samples was three samples, respectively.

**Evaluation of *in vivo* bone response and biodegradation**. New Zealand white rabbits (10 weeks old and 2.8–3.0 kg; KOSA Bio, Korea) were used to evaluate the *in vivo* bone response and biodegradation of the bare Mg, the PEI-coated Mg, and the Ta/PEI-coated Mg cylindrical samples. The preparation method was the same as that mentioned in the corrosion evaluation section. The *in vivo* animal experiments were permitted by the Institutional Animal Care and Use Committee of Genoss Co. Ltd. (GEN-IACUC no. 1811-03). The *in vivo* animal tests were performed using the rabbit femoropatellar groove model [38]. All rabbits were anesthetized by an anesthetic mixture with 0.7 mL of 2% xylazine hydrochloride (HCl; Rompun, Bayer Korea, Korea), 1.4 mL of tiletamine HCl (Zoletil, Virbac Laboratories, France), and 0.5 mL of Lidocaine (Yuhan Corporation, Korea) administered by intramuscular injection. Following anesthetization, a cylindrical hole (4 mm in diameter and 6 mm in length) was formed in the femoral groove parallel to the long axis of the femur using a hand drill. The bare Mg, the PEI-coated Mg, and the Ta/PEI-coated Mg cylindrical samples were individually implanted into the said hole (Figure S1).

The rabbits were sacrificed four weeks post implantation. The corroded volume of and the total bone formation around each Mg sample were assessed by μ-CT scanning of the harvested bone tissues and specimens with a 1-mm aluminum filter at a resolution of 17 μm, a voltage of 130 kV, and a current of 60 μA. The two-dimensional (2D) and 3D images of the samples and bone tissues were reconstructed with post-processing software (NRecon and Data Viewer 1.4, Skyscan). The corroded volume and bone formation volume were quantified using CTAn software with the processed μ-CT images; the 3D images of the samples and bone tissues were acquired using CTVox software. Three samples from each type were used to attain the mean and standard deviation values. Following completion of μ-CT imaging, the extracted regions were fixed using 10% formaldehyde and embedded in resin (Technovit 7200 VLC, Kulzer, Germany). These samples were grinded and sectioned to a thickness of <50 μm using a grinding system (EXAKT, Germany). Histological sections were stained by Goldner's trichrome and analyzed using a panoramic digital slide scanner (Panoramic 250 Flash III, 3DHISTECH Ltd., Hungary).

**Statistical analysis**. Herein, data are presented in the form of mean ± standard deviation. Statistical Package for the Social Sciences software (International Business Machines, USA) was utilized for the statistical analysis. Variable normality was verified using the Shapiro–Wilk test, and the statistical analysis was conducted through one-way variance analysis with Tukey post-hoc comparison. A p-value of less than 0.05 constituted statistical significance for all cases.

## 3. Results

**Surface characterization**. The surface morphologies and chemical compositions of each samples are shown in Fig. 1B–D, from which it is evident that the bare Mg has distinct grinding grooves distributed evenly throughout the surface (Fig. 1Ba); in contrast, completely smooth surface morphologies can be observed on the PEI-coated and Ta/PEI-coated Mg without any noticeable surface defects (Fig. 1Bb–c). As shown in the insets of Fig. 1Bb–c, both coating layers have an almost identical thickness of 2 μm; moreover, they are both uniformly coated on the Mg surface with good interfacial adhesion (Figure S2). The average surface roughness of the bare Mg ($R_a = 33.2 \pm 7.2$ nm) is roughly 25.5 and 19.5 times larger than those of the PEI-coated Mg ($R_a = 1.3 \pm 0.3$ nm) and Ta/PEI-coated Mg ($R_a = 1.7 \pm 0.6$ nm), respectively (Fig. 1Ca–c and Table S1). Furthermore, no statistical differences exist between the PEI-coated and Ta/PEI-coated Mg ($p > 0.05$). The elemental compositions of the surface of PEI-coated Mg and Ta/PEI-coated Mg were determined via EDS mapping, as shown in Table S2 and Figure S3. The results show the presence of C, O, N, and Mg (Figure S3a) in the PEI-coated Mg, whereas an additional Ta peak with 0.21 at.% was detected in Ta/PEI-coated Mg (Table S2 and Figure S3b). To further demonstrate the chemical composition of each surface, XPS analysis was conducted. As shown in Fig. 1Da–b and Table S3, the PEI-coated Mg has representative peaks of PEI chemical elements, including C 1s, O 1s, and N 1s; moreover, the peaks of Mg (Mg 2p and KLL) completely disappear from the spectrum [24,38]. Contrastingly, for the Ta/PEI-coated Mg in Fig. 1Dc, three peaks of PEI can still be observed alongside additional peaks of metallic Ta (Ta 4f and 4d). In the high-resolution spectrum of Ta 4f (top-right inset of Fig. 1Dc), high-intensity peaks of $Ta_2O_5$ at binding energies of 26.3 and 28.3 eV [39] and low-intensity peaks of $Ta^0$ at 21.5 and 23.4 eV can be observed [40].

Cross-sectional TEM analysis suggests that the Ta-implanted nanolayer was constructed on the topmost surface of the PEI coating with a depth of roughly 10 nm; the bright section shown in Fig. 2a can be attributed to the relatively high atomic weight of the implanted Ta. Furthermore, the EDS elemental line profiles suggest that the Ta and O have a parabolic distribution at this depth; their atomic percentages increase and then gradually decrease after attaining maximum amounts of 20 and 60 at.%, respectively, with a decrease in depth below the surface (Fig. 2b).

Adhesion strengths of the PEI- and Ta/PEI-coating layers on the Mg substrate were measured through the pull-out test. As shown in Figure S4a, both coating layers have an almost identical adhesion strength to the Mg substrate with no statistical difference ($p > 0.05$); the average adhesion strength of the PEI coating is 14.2 ± 0.9 MPa, which is well-matched with the reported data [35], and following Ta S-PIII treatment, the Ta/PEI coating exhibited an adhesion strength of 13.7 ± 2 MPa. Following the pull-out test, both coating layers underwent adhesion failure that occurred at the coating/substrate interface, demonstrating that debonding was a smooth process (Figure S4b).

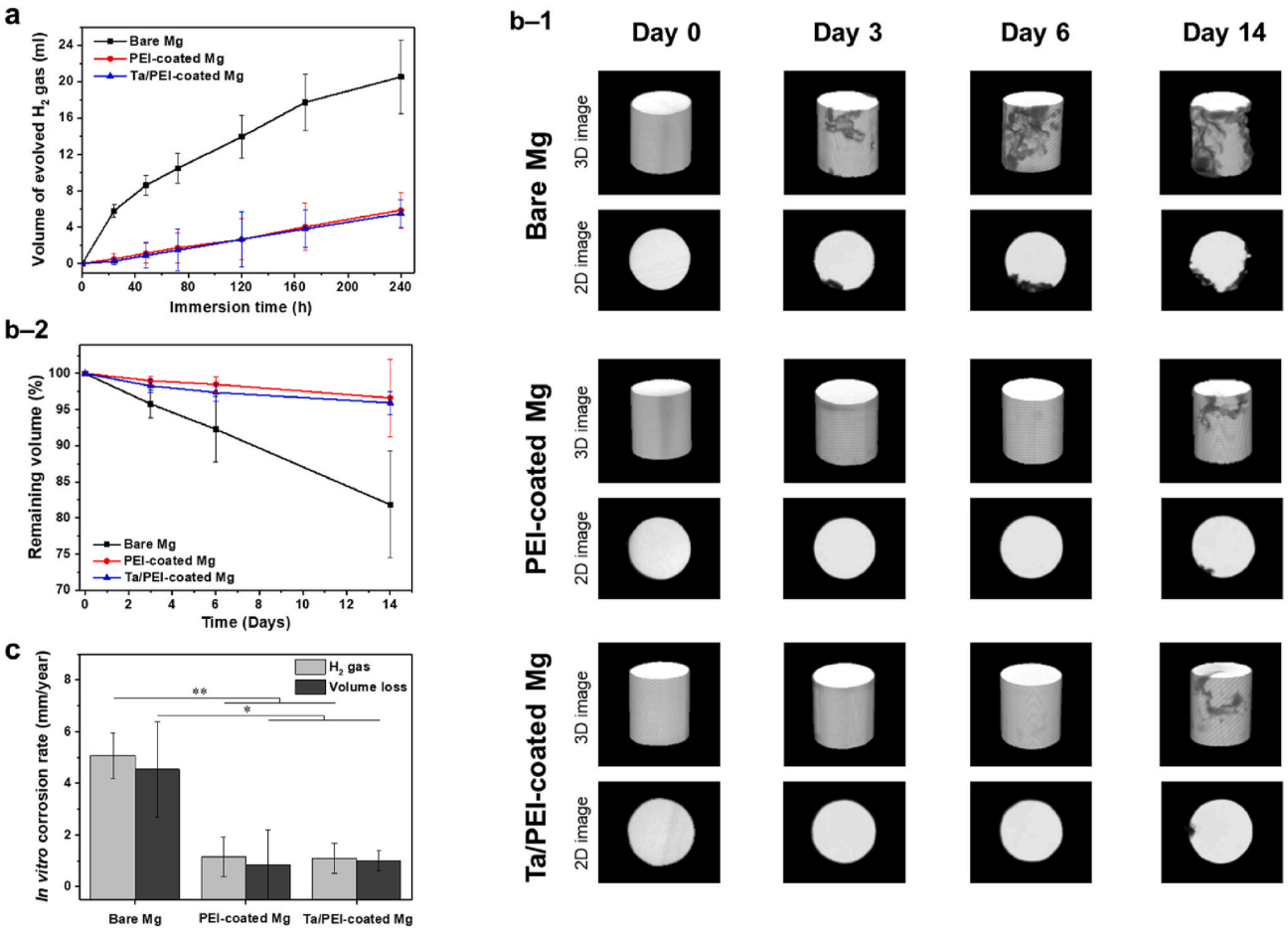


**Fig. 3.** (a) Evolved $H_2$ gas after immersion in SBF solution of bare, PEI-coated, and Ta/PEI-coated Mg samples for 10 days. μ-CT characterization of bare, PEI-coated, and Ta/PEI-coated Mg implants after 14 days of immersion in SBF solution: (b-1) 3D images of each implant at 0, 3, 6, and 14 days of immersion and their (b-2) remaining volumes. (c) The implants' calculated corrosion rates. Statistical significance is indicated by *p < 0.05 and **p < 0.01 compared with bare Mg.

**Corrosion behavior of the tantalum/poly(ether imide)-coated magnesium implant.** The amount of $H_2$ gas, one of the major byproducts of Mg corrosion, generated from the surface of the bare, PEI-coated, and Ta/PEI-coated Mg samples was measured under the SBF immersion condition. As shown in Fig. 3a, the bare Mg rapidly corroded with drastically increased levels of $H_2$ gas evolution; the total amount of gas exceeded 20 mL. Contrastingly, the PEI-coated Mg and Ta/PEI-coated Mg demonstrated significantly reduced corrosion rates compared with the bare Mg; $H_2$ gases were steadily (but much more gradually) generated from both surfaces, resulting in almost linear profiles for the overall immersion time; the total amount of gas for both was roughly 6 mL. Furthermore, hydroxyl ions, which are also a byproduct of Mg corrosion, increase the pH of SBF during corrosion. As shown in Figure S5, from the bare Mg, the pH rapidly increased from 7.3 to ~9.2. The PEI-coated Mg and Ta/PEI-coated Mg exhibited a rise in the pH of SBF of ~7.6, indicating that the PEI coating effectively reduced the corrosion rate of the Mg.

Fig. 3b shows the structural changes and remaining volumes of each Mg sample up to 14 days of immersion in the SBF solution. In the reconstructed μ-CT images (Figs. 3b–1), the bare Mg corrosion proceeded locally; its outer surface suffered from deep and narrow cavities after three days of immersion. As the immersion time increased, the corrosion increased in depth and width, resulting in rough and irregular surface morphologies after 14 days. In contrast, the PEI-coated and Ta/

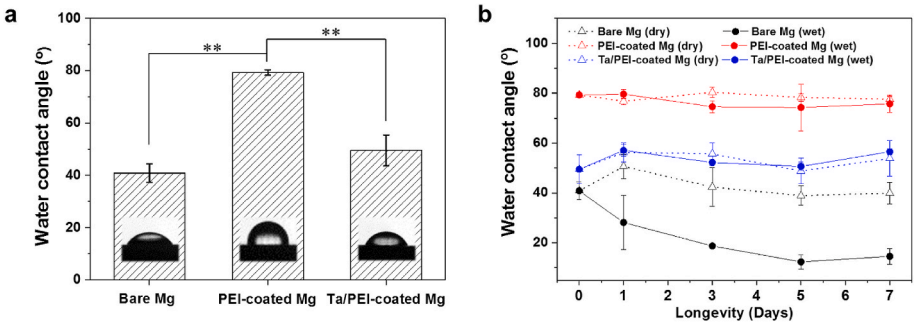


**Fig. 4.** (a) Water contact angles of bare, PEI-coated, and Ta/PEI-coated Mg samples and (b) their longevities as a function of time under air and PBS immersion conditions (**p < 0.01).

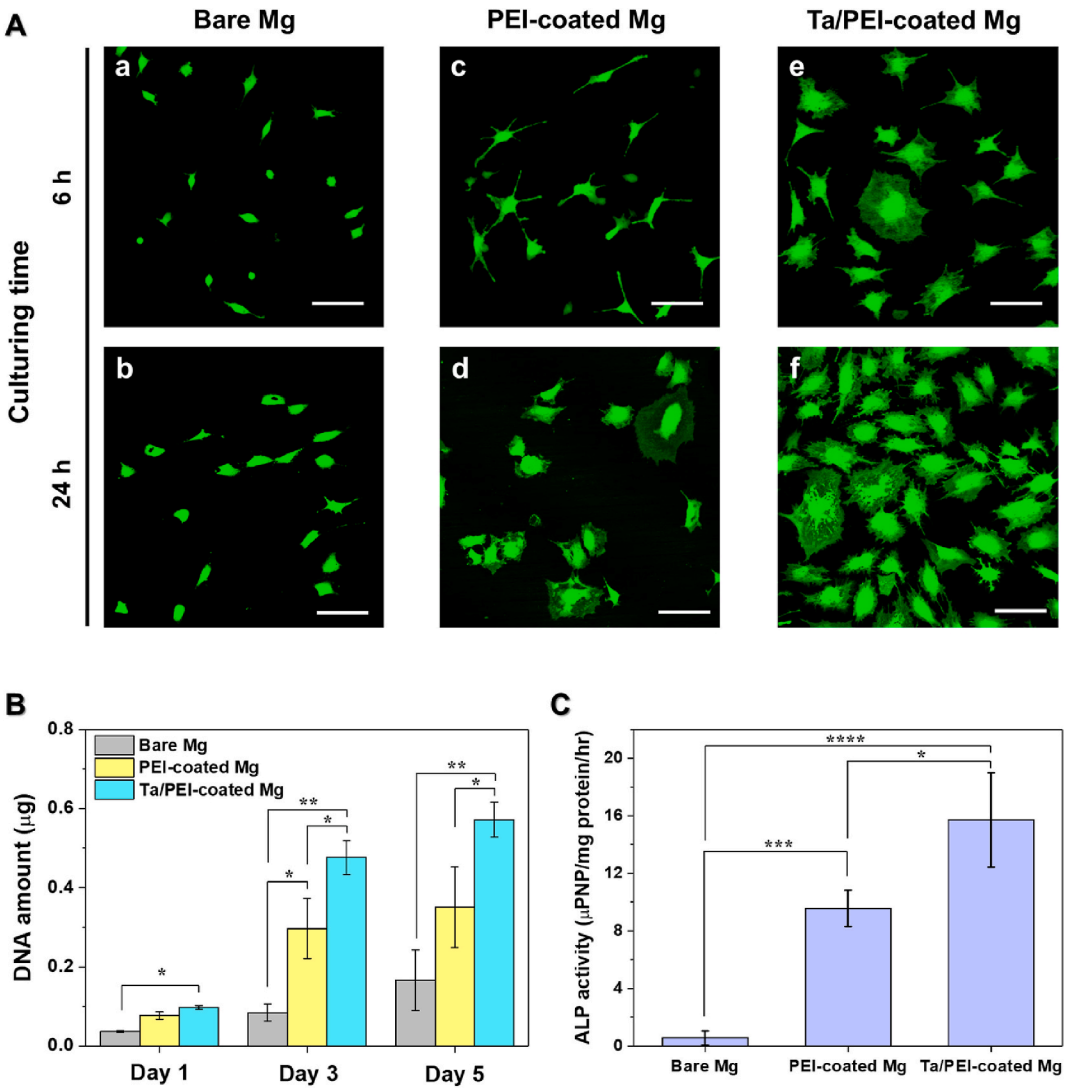


**Fig. 5.** (A) CLSM images of adhered MC3T3-E1 cells on the surface of (a)–(b) bare, (c)–(d) PEI-coated Mg, and (e)–(f) Ta/PEI-coated Mg after culturing for 6 and 24 h (scale bar: 100 μm). (B) DNA amount and (C) ALP activity of MC3T3-E1 cells on each sample after culturing for 1, 3, and 5 days and 10 days, respectively (*$p < 0.05$, **$p < 0.01$, ***$p < 0.005$, and ****$p < 0.001$).

PEI-coated Mg surfaces were essentially pristine with no visible corrosion observed after six days of immersion; post 14 days, the corrosion was still minimal and almost nonexistent. The quantitative results (Figs. 3b–2) show a consistency between the morphometric analysis and the measured remaining volume of the Mg samples. Obviously, the PEI-coated Mg and Ta/PEI-coated Mg lost volume at a slower rate than the bare Mg, showing slight volume losses of 3.2% ± 5.5% and 4.1% ± 1.6%, respectively, whereas the bare Mg only had 81.8% ± 7.4% of volume remaining after 14 days of immersion. Indeed, significant differences cannot be observed with respect to the corrosion protection ability of the PEI-coated and Ta/PEI-coated Mg samples.

Fig. 3c shows the material losses as average *in vitro* corrosion rates for the Mg substrates calculated from the $H_2$ gas evolution measurement and μ-CT characterization. Markedly, the bare Mg has a significantly faster corrosion rate (5.08 ± 0.89 mm/year from the $H_2$ gas evolution measurement and 4.5 ± 1.2 mm/year from the μ-CT characterization) compared with the PEI-coated Mg (1.16 ± 0.75 and 1.02 ± 1.23 mm/year, respectively) and Ta/PEI-coated Mg (1.09 ± 0.58 and 1.05 ± 0.23 mm/year, respectively). No statistical differences exist between both measurements ($p > 0.05$).

**Surface wettability.** Prior to investigating the cellular responses of the bare Mg, PEI-coated Mg, and Ta/PEI-coated Mg, surface wettability was evaluated by conducting water contact angle measurements, which is one of the most important material properties with respect to cell adhesion and growth as well as tissue development. This is shown in Fig. 4a. Although the bare Mg surface exhibited moderate hydrophilicity with a contact angle of 40.8 ± 3.6°, the PEI-coated Mg had a significantly increased surface hydrophobicity with a contact angle of 79.3 ± 1.1°, which is consistent with previously published data [41], as shown in Table S4·In contrast, following the S-PIII treatment, the Ta/PEI-coated Mg exhibited similar wettability to the bare Mg, with a contact angle of 49.5 ± 5.9°; this surface hydrophilicity remained almost constant for seven days under both air and PBS immersion conditions (Fig. 4b), suggesting long-term surface hydrophilicity. As the bare Mg rapidly corroded under the wet condition owing to the formation of porous corrosion byproducts of $Mg(OH)_2$ and MgO [24,38,42], its water contact angle significantly decreased with an increase in immersion time to 12.3 ± 2.8°.

***In vitro* biological evaluation.** The biological response of the pre-osteoblast cells on the bare Mg, PEI-coated Mg, and Ta/PEI-coated Mg surfaces was assessed through *in vitro* cell tests, including cell adhesion, proliferation, and differentiation. Fig. 5A shows the typical CLSM images of adhered cells on each Mg surface that were cultured up to 24 h and stained using a live-cell staining assay. Indeed, the bare Mg has poor

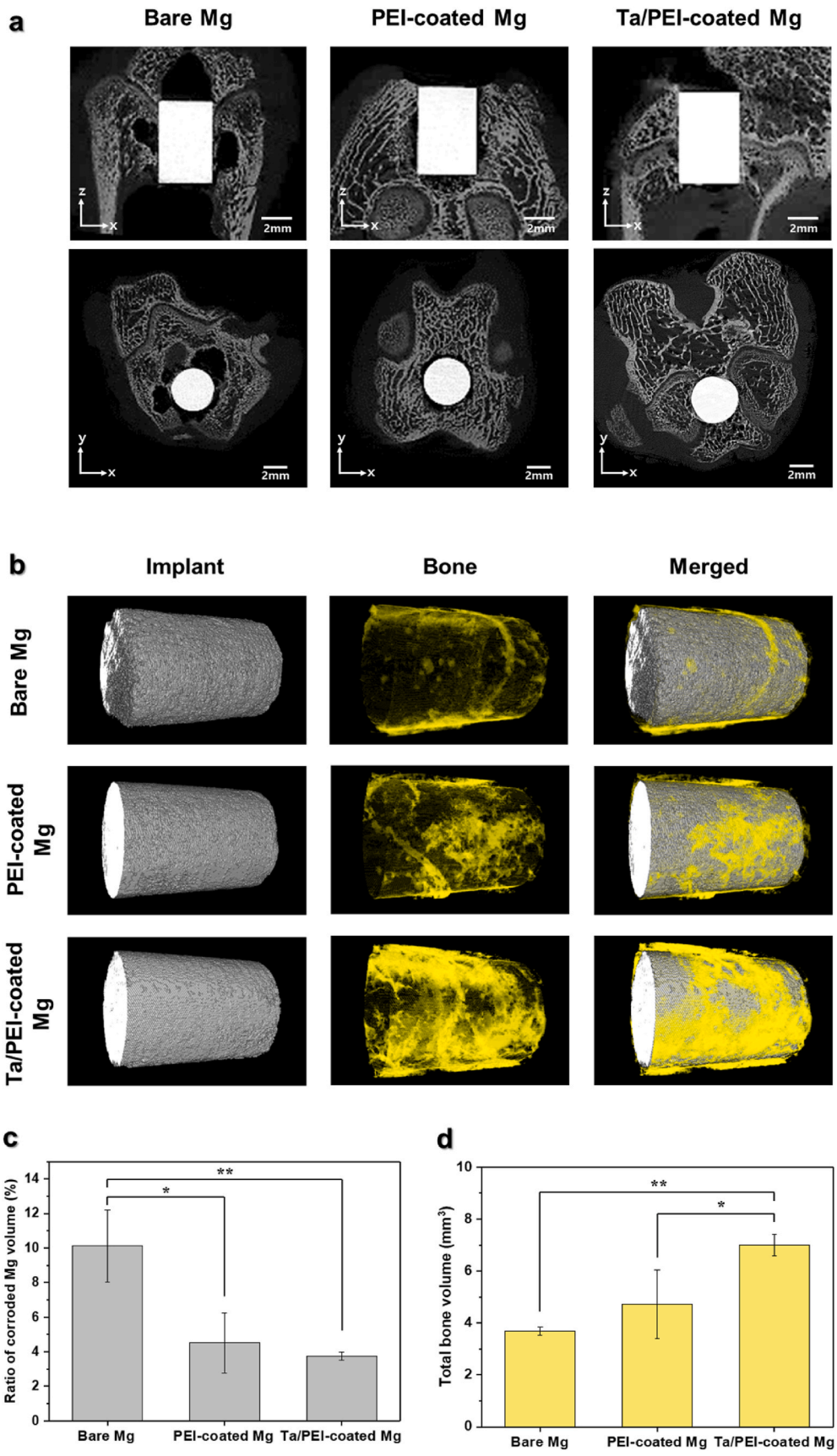


**Fig. 6.** μ-CT characterization of implanted bare, PEI-coated, and Ta/PEI-coated Mg samples and their surrounding bones four weeks post implantation: (a) 2D coronal and transverse views of implants and (b) 3D images of each implant in rabbit femurs, (c) ratio of corroded Mg volume, and (d) total bone volume within a defined region.

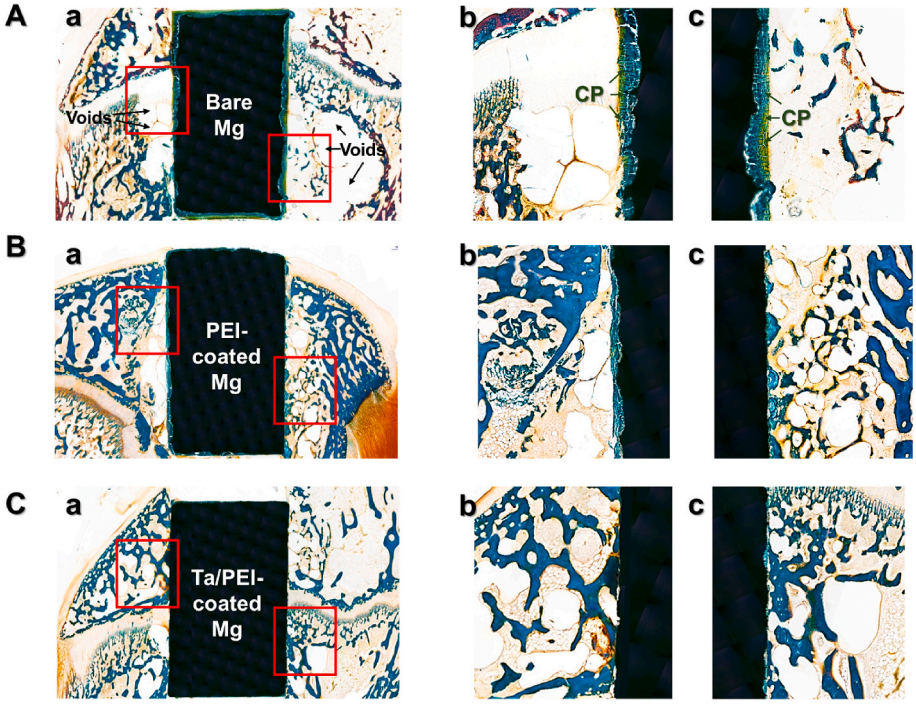


**Fig. 7.** Representative histological images of (A) bare, (B) PEI-coated, and (C) Ta/PEI-coated Mg implants with (a) small and (b)–(c) large magnifications around the implantation regions for rabbit femur four weeks post-surgery. Magnified regions are marked with red rectangles in relatively low-magnification images.

cell-spreading ability for the pre-osteoblasts; most cells retained their round morphologies and did not spread over the bare Mg surface during the culture period (Fig. 5Aa–b). In addition, the number of adhered cells essentially did not change between 6 and 24 h. In contrast, for the PEI-coated Mg surface, the cells formed distinct filopodia-like protrusions extending in multiple directions (Fig. 5Ac). With an increase in culturing period, they firmly adhered to the PEI-coated Mg surface with better spreading abilities and more flattened cell morphologies than the cells on the bare Mg surface (Fig. 5Ad). However, the PEI-coated Mg surface had a similar number of adhered cells as the bare Mg during the 24 h of culturing, suggesting no significant increase in cell number at early time points. For the Ta/PEI-coated Mg surface, the cells had the most pronounced morphological response to the surface out of all samples for all time points. Following 6 h of culturing, the cells were flattened and spread out with a significant number of filopodia- and lamellipodia-like protrusions (Fig. 5Ae). After 24 h, they progressively proliferated on the surface and covered a large area (Fig. 5Af).

Cell proliferation and differentiation were evaluated by measuring the DNA amount and the ALP activity of the pre-osteoblasts on the bare Mg, PEI-coated Mg, and Ta/PEI-coated Mg surfaces at different time points. As shown in Fig. 5B, for the PEI-coated and Ta/PEI-coated Mg surfaces, the amount of DNA significantly increased with an increase in culturing time, whereas, for the bare Mg surface, the amount of DNA increased but not significantly. In particular, the Ta/PEI-coated Mg had the highest rate of pre-osteoblast proliferation: 590% and 160% higher levels on the third day and 343% and 162% higher levels on the fifth day compared with the bare Mg and PEI-coated Mg surfaces, respectively. The ALP activity levels, an early indicator of osteogenic differentiation, are shown in Fig. 5C. Although the bare Mg had almost no osteogenic ability with a value of $0.55 \pm 0.49$, the PEI-coated Mg surface saw an increase in ALP activity. For the Ta/PEI-coated Mg surface, the level of ALP activity further increased, showing 2856% and 164% higher values compared with the bare and PEI-coated Mg surfaces.

***In vivo* biodegradation and biological evaluation**. To assess the *in vivo* biodegradability and osteogenic capability of the materials, cylinder-shaped bare, PEI-coated, and Ta/PEI-coated Mg samples were implanted in both sides of the femoropatellar defects for each rabbit; after four weeks, the implanted samples and trabecular bones around the sample were evaluated through μ-CT, as shown in Fig. 6. The 2D coronal and transverse images of the implanted samples clearly show the adverse biological reaction of the bare Mg implant (Fig. 6a): extremely large voids around the implant surfaces; surrounding trabecular bone tissues are completely separated from the implant surface, leaving the implant almost unfixed in the host femur. In the reconstructed μ-CT images (Fig. 6b), the bare Mg has a considerably corroded and rough surface with deep corrosion pits and dents as well as small amounts of thin bone layers. In contrast, the PEI-coated and Ta/PEI-coated Mg samples have better bone formation and corrosion resistance than the bare Mg: no sign of noticeable corrosion damage on the surface and surrounding trabecular bone tissue; surfaces mostly covered with newly formed bone tissue (Fig. 6a and b). In particular, the Ta/PEI-coated Mg exhibits outstanding bone tissue compatibility as it has the most extensive and thickest bone formation among all samples. As shown in Fig. 6c, the volume reductions of the PEI-coated and Ta/PEI-coated Mg implants decreased by roughly 4%, whereas the volume reduction of the bare Mg decreased by 10%. Consequently, the *in vivo* corrosion rates of the PEI-coated and Ta/PEI-coated Mg implants are less than that of the bare Mg. In addition, as shown in Fig. 6d, the Ta/PEI-coated Mg has statistically significant bone formation compared with the bare ($p < 0.01$) and PEI-coated Mg implants ($p < 0.05$).

Histological images for the bare, PEI-coated, and Ta/PEI-coated Mg implants are shown in Fig. 7; the longitudinally sectioned implants were stained with Goldner's trichrome. Mineralized and matured bone is represented by dark green, newly formed but still unmineralized bone (osteoid) is represented by orange, and the Mg implants are represented by light green (for corrosion product) and black (for the not yet corroded matrix). Overall, the bare Mg implant has a severely corroded surface with increased amounts of corrosion byproducts compared with the coated Mg implants. In particular, as indicated by the voids in Fig. 7Aa–c, vigorous $H_2$ gas evolution surrounds the bare Mg implant, which can explain the complete separation of the trabecular bone from the implant surface. In case of the PEI-coated and Ta/PEI-coated Mg implants, at low magnification, neither appreciable corrosion can be observed nor void formation around the implant (Fig. 7Ba and Ca); at

high magnification, minimal amounts of corrosion byproducts can be observed (Fig. 7Bb–c and Cb–c). Although some sections of the trabecular bone in the distal femur were not in contact with the surface of the PEI-coated Mg, thereby resulting in tissue-free voids around the implant, the Ta/PEI-coated Mg implant remained tightly adhered to the adjacent bone tissue; moreover, a larger portion of its surface was surrounded by trabecular bones instead of voids. Additionally, much of the mineralized and unmineralized bones were in direct contact with, or close to, the Ta/PEI-coated Mg implant surface.

## 4. Discussion

In the field of orthopedic biomedical materials, addressing the clinical challenges of suppressing the rapid corrosion and achieving the osseointegration ability of Mg implants have attracted considerable research attention [1,6,43,44]. Although considerable efforts have been made in polymeric coating technologies to address corrosion problems, the development of advanced surface treatment techniques to address both challenges is still ongoing [19,45]. Herein, a PEI-coating layer provides outstanding corrosion protection to the Mg implant owing to its innate hydrophobicity and stable adhesiveness to the Mg. However, according to the *in vivo* results, the PEI-coated Mg does not show any evidence of direct bone-to-implant contact around the implant surface. Therefore, modifying the surface of the polymer coatings to alter their physical and chemical characteristics without deteriorating their intrinsic corrosion protection abilities is necessary.

The S-PIII technique is able to generate numerous Ta ions from the sputtering target, subsequently implanting them on the topmost surface of polymeric substances at markedly high doses [25]. Indeed, this unique characteristic enables drastic reduction in the time required to modify the PEI surface to 30 s, thereby minimizing the possibility of coating damage and loss of adhesion stability (Figure S2 and S4). Based on the surface morphology observations and roughness measurements, any differences between the PEI-coated and the Ta/PEI-coated Mg are not obvious. In particular, after the S-PIII surface treatment, the PEI coating preserved its original smooth surface features without any signs of ion implantation damage (Fig. 1B); moreover, it exhibited negligible changes in surface roughness (Fig. 1C and Table S1). In contrast, the surface XPS (Fig. 1D) and cross-sectional STEM elemental analysis (Fig. 2a and b) indicate the development of a Ta-implanted layer on the topmost surface of the PEI coating. Even with its short processing time, the extremely high negative bias voltage (−2 kV) applied to the Mg substrate was highly effective in inducing energetic Ta ion irradiation and implantation onto the PEI surface though building up an ion sheath around the Mg implant. Therefore, a considerable amount of Ta was successfully implanted from the top surface of the PEI to a depth of roughly 10 nm; it did not make a physical interface with the PEI coating, suggesting structural stability under physiological conditions. Additionally, a large amount of this Ta was combined with oxygen when undergoing the S-PIII process (Table S3), forming a stable and passive layer of $Ta_2O_5$, which is known to strongly interact with the imide ring of PEI molecules, in addition to beneficially affecting the osteoblasts, thereby ensuring intimate contact with the bone [46]. Therefore, the S-PIII surface treatment with Ta can effectively solve the problem of deficient osseointegration of PEI-coated Mg implants.

From the $H_2$ gas evolutions, the pH variation and volume reduction measurements in SBF solution shown in Fig. 3 and S5, it is evident that the PEI-coated Mg and Ta/PEI-coated Mg have nearly identical corrosion resistance, with little statistical difference ($p > 0.05$). When compared to the bare Mg, those corrosion rates are significantly lower (by a factor of five) and are almost linear. The calculated $H_2$ release rates of PEI-coated Mg and Ta/PEI-coated Mg were 0.58 ± 0.19 and 0.55 ± 0.15 mL/cm$^2$/day, respectively, and were approximately one fourth that of bare Mg (2.04 ± 0.40 mL/cm$^2$/day). The critical rate of $H_2$ release depends on various factors such as the object's size, type, and condition. One study showed that the acceptable $H_2$ release rate of the guinea pig is 0.01 mL/cm$^2$/day [47], whereas another study suggested that the tolerable adsorption rate of $H_2$ for the human body is 2.25 mL/cm$^2$/day [48]. Comparing the *in vitro* results reported herein, we found that $H_2$ evolution rates of both PEI-coated Mg and Ta/PEI-coated Mg are significantly lower than the tolerance level of the human body. Typically, polymeric coating layers effectively reduce the extremely high activity of Mg by thermodynamically controlling the rate-determining step of the overall corrosion reaction [17,49]. In essence, hydrophobic and dense polymer matrices substantially retards the penetration of a corrosive medium to the Mg substrate, slowing the slowest step of all kinetic corrosion processes, and, consequently, decreases the corrosion rate [49]. Although the Ta ion implantation altered the physical and chemical properties of the PEI coating, the Ta-implanted layer was only a few tens of nanometers thick, which is probably too shallow for the PEI coating to alter the overall corrosion protection. Moreover, Ta and $Ta_2O_5$ exhibit very good corrosion resistance, and are known to suppress corrosion in corrosive solutions such as bodily fluids by coating and protecting the surface of the metallic substrate [50]. Additionally, Li et al. [51] explained that a $Ta_2O_5$ film can act as a physical barrier in a corrosive medium and can prevent the corrosion of the Mg substrate by blocking the penetration of aggressive ions, such as $Cl^-$, which cause Mg corrosion. Based on these reports, the $Ta_2O_5$ region formed on the top of the PEI coating layer will have prevented the penetration of solutions or other ions. Although the penetration of water may be increased by a Ta-metallized surface, ion penetration is suppressed. As a result of this synergetic effect, the corrosion resistance is not significantly altered.

In contrast, compared with the PEI coating, the *in vitro* studies clearly demonstrated that the Ta-implanted PEI-coating layer can improve the pre-osteoblast responses toward the Mg implants. Compared with bare Mg, the PEI-coated Mg has enhanced pre-osteoblast viability and osteogenic differentiation because the PEI layer prevents rapid Mg corrosion and suppresses the production of $H_2$ gases and hydroxyl ions (Fig. 5B–C). Furthermore, alkalization by Mg corrosion can also affect cellular responses. Galow et al. suggested that when the pH is higher than 8.4, the proliferation and differentiation of osteoblasts is reduced. However, in the intermediate pH range of 7.4–8.4, it has been shown that the proliferation and differentiation of osteoblasts increases along with the increasing pH value [52]. Similarly, Kaysinger and Ramp et al. proposed that osteoblastic activity increases with increasing pH in the range of 7.0–7.6 [53]. The PEI-coated Mg and Ta/PEI-coated Mg had a positive effect on osteoblast viability because the pH increased to about 7.6 during *in vitro* corrosion testing, whereas the cell viability of osteoblasts on the uncoated Mg was inhibited, with a very low amount of proliferation and differentiation activity, as shown in Fig. 5. However, its lack of surface functionalities and long-term hydrophobic surface characteristic are not favorable for early pre-osteoblast cell adhesion and spreading. This is evident from the fact that, after 24 h of culturing, spherical cell bodies were retained, remaining essentially unchanged (Fig. 5A). In contrast, the S-PIII treatment effectively ameliorated the surface hydrophobicity of the PEI coating, demonstrating a water contact angle reduction of 38% compared with the bare Mg and PEI-coated Mg, a value that remained essentially constant under dry and wet conditions (Fig. 4). During the S-PIII treatment, massive Ta ion implantation can result in various PEI structures, such as chain scission, recombination, and imide ring degeneration, as well as subsequent chemical adsorption of oxygen onto the surface, thereby forming highly reactive functional groups [54]. These oxygen functionalities combine with implanted Ta elements that have smaller water contact angles than pristine PEI (Figure S6 and Table S4), which subsequently renders the PEI surface more hydrophilic and ensures access to cell-containing media and nutrients. In addition, as Ta is one of the most biocompatible and bioactive metals, the Ta-implanted surface layer provided numerous binding sites on the surface for the pre-osteoblasts to adhere to and spread from Ref. [25,32,55], resulting in abundant formations of filopodia-like cell protrusions on the Ta/PEI-coated Mg (Fig. 5A). Typically, cells are actively sensing and signaling their microenvironments through the

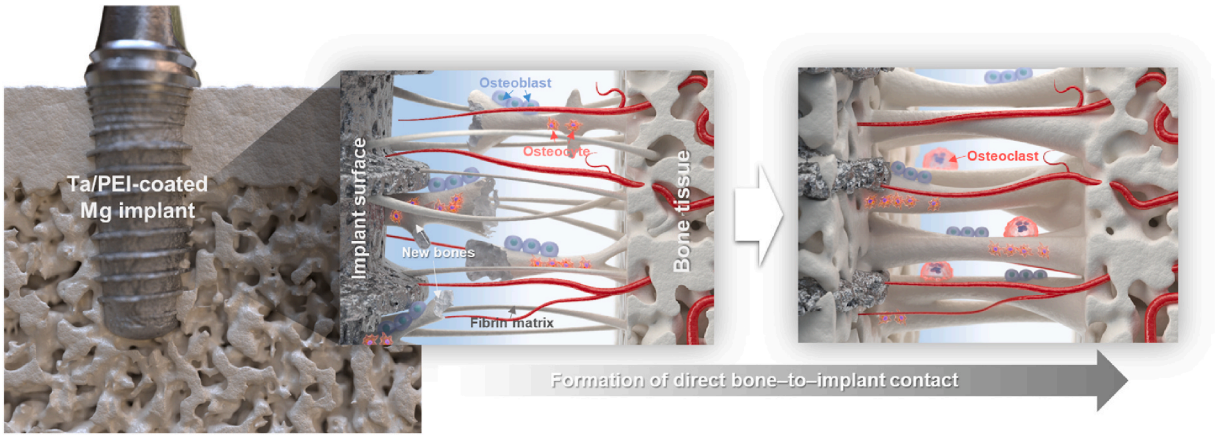


**Fig. 8.** Schematic of the process of Ta/PEI-coated Mg implant osseointegration.

formation of filopodia, which directly stimulate the focal adhesion assembly and extension of lamellipodia [56,57]. Therefore, these active cell–surface interactions on the Ta/PEI-coated Mg are responsible for the highest levels of cell proliferation and osteogenic differentiation among the samples (Fig. 5B–C) [58].

The *in vivo* rabbit femur study also clearly demonstrates the excellent corrosion protection ability of the PEI coating and the osseointegration ability of the Ta-implanted surface layer. Without the PEI coating, the bare Mg rapidly corroded; its surface was rough with thick corrosion byproducts (Fig. 7A). In addition, the rapid and continuous development of $H_2$ gases and hydroxyl ions on the surface of the Mg implant significantly reduced total bone volume and resulted in large voids (Fig. 6a). Indeed, the introduction of the PEI-coating layer sufficiently reduced the *in vivo* corrosion rate of the bare Mg and enhanced trabecular bone formation around the surface, thereby reducing the corrosion rate by 45% and increasing the total bone volume by 130% (Fig. 6c and d). However, from the histological observation, direct bone-to-implant contact did not occur on the surface of the PEI-coated Mg implant (Fig. 7B). Because the primary function of orthopedic implants is to support mechanical loading and replace the biological function of bone, appropriate early fixation and long-term implantation success cannot be achieved in the absence of direct bonding [59,60]. As shown in Fig. 7, among the three samples, the Ta/PEI-coated Mg implant saw direct bone-to-implant contact at the microscopic level; moreover, it saw the highest level of total bone volume around the implant surface, specifically 194% and 149% higher than that of the bare and PEI-coated Mg implants, respectively (Fig. 6c and d). This can mainly be attributed to the presence of Ta. When in contact with body fluids, Ta forms hydroxide groups on the surface, which subsequently attracts calcium and phosphate ions in the body fluid near the surface and ultimately results in the formation of apatite layers [25]. Thus, based on the outstanding corrosion protection ability and biological activity, the Ta/PEI-coated Mg implant has enhanced bone tissue affinity and osseointegration capability (Fig. 8).

## 5. Conclusion

In this study, we introduced a novel approach to modify the surface physical and chemical properties of a polymer-coated Mg implant. The PEI-coated Mg implants demonstrated excellent corrosion protection ability owing to the hydrophobic surface property of the PEI-coating layer and its stable adhesiveness to the Mg surface; however, they did not show any evidence of osseointegration with the surrounding bone. A rapid PIII technique combined with DC magnetron sputtering enabled the introduction of biologically compatible metal ions (Ta) onto the surface of the PEI coating in an extremely short processing time (30 s), thereby creating the Ta/PEI-coated Mg. Indeed, the Ta/PEI-coated Mg did not have any noticeable surface damages; it also exhibited enhanced corrosion protection properties. Moreover, the Ta layer significantly enhanced the surface hydrophilicity and ensured long-term stability under dry and wet conditions. Compared with the bare Mg and PEI-coated Mg, the Ta/PEI-coated Mg was more favorable with respect to the pre-osteoblasts adhering, proliferating, and differentiating, which can be attributed to the bioactivity and biocompatibility of the Ta. In the *in vivo* rabbit femur study, the Ta/PEI-coated Mg implant exhibited enhanced bone tissue affinity and osseointegration capability with no signs of appreciable Mg corrosion. These results suggest that the Ta/PEI-coated Mg is highly suitable as a biodegradable orthopedic implant material.

## Associated content

**Supporting Information**. Photographs of surgical site and the implanted Mg in rabbit distal femurs (Figure S1). Cross-sectional SEM images (Figure S2). EDS mapping, FE-SEM image (Figure S3). Adhesion strength of PEI coating (Figure S4). Surface roughness parameters (Table S1), EDS elemental compositions (Table S2), XPS elemental compositions (Table S3), pH variation (Figure S5), water contact angles (Figure S6 and Table S4).

## Author information

**Author Contributions**. H.E.K. and T.S.J. developed the concept. K. H.C. and H.D.J. designed the experiments. K.H.C., C.P., M.H.K., H.L., and I.G.K. performed the surface characterization analysis, and K.H.C., M.H.K., and M.K.L. performed the *in vitro* cellular experiments. All authors analyzed the data. K.H.C., H.D.J., and T.S.J. wrote the manuscript.

**Notes**. The authors declare no competing financial interests.

## CRediT authorship contribution statement

**Kwang-Hee Cheon:** Methodology, Formal analysis, Writing - original draft. **Cheonil Park:** Formal analysis. **Min-Ho Kang:** Formal analysis. **In-Gu Kang:** Formal analysis. **Min-Kyu Lee:** Formal analysis. **Hyun Lee:** Formal analysis. **Hyoun-Ee Kim:** Conceptualization, Formal analysis. **Hyun-Do Jung:** Writing - original draft, Methodology, Formal analysis. **Tae-Sik Jang:** Conceptualization, Formal analysis, Writing - original draft.

## Declaration of competing interest

This manuscript has not been published or presented elsewhere in part or in entirety and is not under consideration by another journal. We have read and understood your journal's policies, and we believe that

neither the manuscript nor the study violates any of these. There are no conflicts of interest to declare.

## Acknowledgment

This research was supported by a grant of the Korea Health Technology R&D Project through the Korea Health Industry Development Institute (KHIDI), funded by the Ministry of Health & Welfare, Republic of Korea (grant number: HI18C0493).

## Appendix A. Supplementary data

Supplementary data to this article can be found online at https://doi.org/10.1016/j.bioactmat.2020.10.007.

## References

[1] M.P. Staiger, A.M. Pietak, J. Huadmai, G. Dias, Magnesium and its alloys as orthopedic biomaterials: a review, Biomaterials 27 (9) (2006) 1728–1734.
[2] J.C. Middleton, A.J. Tipton, Synthetic biodegradable polymers as orthopedic devices, Biomaterials 21 (23) (2000) 2335–2346.
[3] Y. Yang, J. Zhou, Q. Chen, R. Detsch, X. Cui, G. Jin, S. Virtanen, A.R. Boccaccini, In vitro osteocompatibility and enhanced biocorrosion resistance of diammonium hydrogen phosphate-pretreated/poly(ether imide) coatings on magnesium for orthopedic application, ACS Appl. Mater. Interfaces 11 (33) (2019) 29667–29680.
[4] R. Karunakaran, S. Ortgies, A. Tamayol, F. Bobaru, M.P. Sealy, Additive manufacturing of magnesium alloys, Bioact. Mater. 5 (1) (2020) 44–54.
[5] C.-Y. Li, C. Yu, R.-C. Zeng, B.-C. Zhang, L.-Y. Cui, J. Wan, Y. Xia, In vitro corrosion resistance of a $Ta_2O_5$ nanofilm on MAO coated magnesium alloy AZ31 by atomic layer deposition, Bioact. Mater. 5 (1) (2020) 34–43.
[6] L. Li, M. Zhang, Y. Li, J. Zhao, L. Qin, Y. Lai, Corrosion and biocompatibility improvement of magnesium-based alloys as bone implant materials: a review, Regenerative Biomater. 4 (2) (2017) 129–137.
[7] S. Shadanbaz, G.J. Dias, Calcium phosphate coatings on magnesium alloys for biomedical applications: a review, Acta Biomater. 8 (1) (2012) 20–30.
[8] F. Witte, V. Kaese, H. Haferkamp, E. Switzer, A. Meyer-Lindenberg, C.J. Wirth, H. Windhagen, In vivo corrosion of four magnesium alloys and the associated bone response, Biomaterials 26 (17) (2005) 3557–3563.
[9] L. Tian, Y. Sheng, L. Huang, D.H. Chow, W.H. Chau, N. Tang, T. Ngai, C. Wu, J. Lu, L. Qin, An innovative Mg/Ti hybrid fixation system developed for fracture fixation and healing enhancement at load-bearing skeletal site, Biomaterials 180 (2018) 173–183.
[10] W. Xu, N. Birbilis, G. Sha, Y. Wang, J.E. Daniels, Y. Xiao, M. Ferry, A high-specific-strength and corrosion-resistant magnesium alloy, Nat. Mater. 14 (12) (2015) 1229–1235.
[11] S. Remennik, I. Bartsch, E. Willbold, F. Witte, D. Shechtman, New, fast corroding high ductility Mg–Bi–Ca and Mg–Bi–Si alloys, with no clinically observable gas formation in bone implants, Mater. Sci. Eng., B 176 (20) (2011) 1653–1659.
[12] F. Witte, J. Fischer, J. Nellesen, H.A. Crostack, V. Kaese, A. Pisch, F. Beckmann, H. Windhagen, In vitro and in vivo corrosion measurements of magnesium alloys, Biomaterials 27 (7) (2006) 1013–1018.
[13] A. Carangelo, A. Acquesta, T. Monetta, In-vitro corrosion of AZ31 magnesium alloys by using a polydopamine coating, Bioact. Mater. 4 (2019) 71–78.
[14] M.-H. Kang, K.-h. Cheon, K.-I. Jo, J.-H. Ahn, H.-E. Kim, H.-D. Jung, T.-S.J.M. Jang, Design, an Asymmetric Surface Coating Strategy for Improved Corrosion Resistance and Vascular Compatibility of Magnesium Alloy Stents, Materials & Design, 2020, 109182.
[15] J. Sun, S. Cai, J. Sun, K. Shen, J. Liu, G. Xu, Ultrasonic aqueous synthesis of corrosion resistant hydroxyapatite coating on magnesium alloys for the application of long-term implant, Ultrason. Sonochem. 58 (2019) 104677.
[16] S. Shen, S. Cai, X. Bao, P. Xu, Y. Li, S. Jiang, G. Xu, Biomimetic fluoridated hydroxyapatite coating with micron/nano-topography on magnesium alloy for orthopaedic application, Chem. Eng. J. 339 (2018) 7–13.
[17] J. Degner, F. Singer, L. Cordero, A.R. Boccaccini, S. Virtanen, Electrochemical investigations of magnesium in DMEM with biodegradable polycaprolactone coating as corrosion barrier, Appl. Surf. Sci. 282 (2013) 264–270.
[18] H.M. Wong, K.W. Yeung, K.O. Lam, V. Tam, P.K. Chu, K.D. Luk, K.M. Cheung, A biodegradable polymer-based coating to control the performance of magnesium alloy orthopaedic implants, Biomaterials 31 (8) (2010) 2084–2096.
[19] L.Y. Li, L.Y. Cui, R.C. Zeng, S.Q. Li, X.B. Chen, Y. Zheng, M.B. Kannan, Advances in functionalized polymer coatings on biodegradable magnesium alloys - a review, Acta Biomater. 79 (2018) 23–36.
[20] K.-H. Cheon, C. Gao, M.-H. Kang, H.-D. Jung, T.-S. Jang, H.-E. Kim, Y. Li, J. Song, A crack-free anti-corrosive coating strategy for magnesium implants under deformation, Corrosion Sci. 132 (2018) 116–124.
[21] Z.-Z. Yin, W.-C. Qi, R.-C. Zeng, X.-B. Chen, C.-D. Gu, S.-K. Guan, Y.-F. Zheng, Advances in coatings on biodegradable magnesium alloys, J. Magnes. Alloys 8 (1) (2020) 42–65.
[22] Y.Q. Zhu, K. Yang, R.Y. Cheng, Y. Xiang, T.W. Yuan, B.N. Sarmento, Y.S. Chen, W. G. Cui, The current status of biodegradable stent to treat benign luminal disease, Mater. Today 20 (9) (2017) 516–529.
[23] P. Chakraborty Banerjee, S. Al-Saadi, L. Choudhary, S.E. Harandi, R. Singh, Magnesium implants: prospects and challenges, Materials (Basel) 12 (1) (2019).
[24] S.B. Kim, J.H. Jo, S.M. Lee, H.E. Kim, K.H. Shin, Y.H. Koh, Use of a poly(ether imide) coating to improve corrosion resistance and biocompatibility of magnesium (Mg) implant for orthopedic applications, J. Biomed. Mater. Res. 101 (6) (2013) 1708–1715.
[25] C. Park, Y.J. Seong, I.G. Kang, E.H. Song, H. Lee, J. Kim, H.D. Jung, H.E. Kim, T. S. Jang, Enhanced osseointegration ability of poly(lactic acid) via tantalum sputtering-based plasma immersion ion implantation, ACS Appl. Mater. Interfaces 11 (11) (2019) 10492–10504.
[26] M. Chen, L. Ouyang, T. Lu, H. Wang, F. Meng, Y. Yang, C. Ning, J. Ma, X. Liu, Enhanced bioactivity and bacteriostasis of surface fluorinated polyetheretherketone, ACS Appl. Mater. Interfaces 9 (20) (2017) 16824–16833.
[27] T. Lu, J. Wen, S. Qian, H. Cao, C. Ning, X. Pan, X. Jiang, X. Liu, P.K. Chu, Enhanced osteointegration on tantalum-implanted polyetheretherketone surface with bone-like elastic modulus, Biomaterials 51 (2015) 173–183.
[28] C. Park, S.W. Lee, J. Kim, E.H. Song, H.D. Jung, J.U. Park, H.E. Kim, S. Kim, T. S. Jang, Reduced fibrous capsule formation at nano-engineered silicone surfaces via tantalum ion implantation, Biomater. Sci. 7 (7) (2019) 2907–2919.
[29] C. Park, S. Park, J. Kim, A. Han, S. Ahn, S.K. Min, H.J. Jae, J.W. Chung, J.H. Lee, H. D. Jung, H.E. Kim, T.S. Jang, Enhanced endothelial cell activity induced by incorporation of nano-thick tantalum layer in artificial vascular grafts, Appl. Surf. Sci. 508 (2020).
[30] D. Mareci, R. Chelariu, D.M. Gordin, G. Ungureanu, T. Gloriant, Comparative corrosion study of Ti-Ta alloys for dental applications, Acta Biomater. 5 (9) (2009) 3625–3639.
[31] B.R. Levine, S. Sporer, R.A. Poggie, C.J. Della Valle, J.J. Jacobs, Experimental and clinical performance of porous tantalum in orthopedic surgery, Biomaterials 27 (27) (2006) 4671–4681.
[32] V.H. Pham, T.S. Jang, H.D. Jung, H.E. Kim, Y.H. Koh, Creation of nanoporous tantalum (Ta)-incorporated titanium (Ti) surface onto Ti implants by sputtering of Ta in Ar under extremely high negative substrate biases, J. Mater. Chem. 22 (47) (2012) 24798–24804.
[33] T.F. Conceicao, N. Scharnagl, C. Blawert, W. Dietzel, K.U. Kainer, Corrosion protection of magnesium alloy AZ31 sheets by spin coating process with poly(ether imide) [PEI], Corrosion Sci. 52 (6) (2010) 2066–2079.
[34] T.F. da Conceicao, N. Scharnagl, W. Dietzel, K.U. Kainer, Corrosion protection of magnesium AZ31 alloy using poly(ether imide) [PEI] coatings prepared by the dip coating method: influence of solvent and substrate pre-treatment, Corrosion Sci. 53 (1) (2011) 338–346.
[35] M.H. Kang, T.S. Jang, H.D. Jung, S.M. Kim, H.E. Kim, Y.H. Koh, J. Song, Poly(ether imide)-silica hybrid coatings for tunable corrosion behavior and improved biocompatibility of magnesium implants, Biomed. Mater. 11 (3) (2016), 035003.
[36] T.-S. Jang, J.H. Lee, S. Kim, C. Park, J. Song, H.J. Jae, H.-E. Kim, J.W. Chung, H.-D. Jung, Ta ion implanted nanoridge-platform for enhanced vascular responses, Biomaterials 223 (2019), 119461.
[37] T. Kokubo, H. Takadama, How useful is SBF in predicting in vivo bone bioactivity? Biomaterials 27 (15) (2006) 2907–2915.
[38] M.H. Kang, H. Lee, T.S. Jang, Y.J. Seong, H.E. Kim, Y.H. Koh, J. Song, H.D. Jung, Biomimetic porous Mg with tunable mechanical properties and biodegradation rates for bone regeneration, Acta Biomater. 84 (2019) 453–467.
[39] E. Atanassova, T. Dimitrova, J. Koprinarova, Aes and xps study of thin Rf-sputtered Ta2o5 layers, Appl. Surf. Sci. 84 (2) (1995) 193–202.
[40] J.Y. Zhang, I.W. Boyd, Thin tantalum and tantalum oxide films grown by pulsed laser deposition, Appl. Surf. Sci. 168 (1–4) (2000) 234–238.
[41] W. Jin, G. Wu, H. Feng, W. Wang, X. Zhang, P.K. Chu, Improvement of corrosion resistance and biocompatibility of rare-earth WE43 magnesium alloy by neodymium self-ion implantation, Corrosion Sci. 94 (2015) 142–155.
[42] D. Zhao, T. Wang, K. Nahan, X. Guo, Z. Zhang, Z. Dong, S. Chen, D.-T. Chou, D. Hong, P.N. Kumta, In vivo characterization of magnesium alloy biodegradation using electrochemical H2 monitoring, ICP-MS, and XPS, Acta Biomater. 50 (2017) 556–565.
[43] Y. Xin, T. Hu, P. Chu, In vitro studies of biomedical magnesium alloys in a simulated physiological environment: a review, Acta Biomater. 7 (4) (2011) 1452–1459.
[44] H.M. Wong, Y. Zhao, F.K. Leung, T. Xi, Z. Zhang, Y. Zheng, S. Wu, K.D. Luk, K. M. Cheung, P.K. Chu, Functionalized polymeric membrane with enhanced mechanical and biological properties to control the degradation of magnesium alloy, Adv. Healthcare Mater. 6 (8) (2017), 1601269.
[45] H. Hornberger, S. Virtanen, A.R. Boccaccini, Biomedical coatings on magnesium alloys–a review, Acta Biomater. 8 (7) (2012) 2442–2455.
[46] M. Grujicic, V. Sellappan, M.A. Omar, N. Seyr, A. Obieglo, M. Erdmann, J. Holzleitner, An overview of the polymer-to-metal direct-adhesion hybrid technologies for load-bearing automotive components, J. Mater. Process. Technol. 197 (1–3) (2008) 363–373.
[47] G.J.C.s. Song, Control of biodegradation of biocompatable magnesium alloys 49 (4) (2007) 1696–1701.
[48] Z. Chun-Yan, Z. Rong Chang, L. Cheng-Long, G.J.S. Jia-Cheng, C. Technology, Comparison of calcium phosphate coatings on Mg–Al and Mg–Ca alloys and their corrosion behavior in Hank's solution, Surf. Coating. Technol. 204 (21–22) (2010) 3636–3640.
[49] Y.Q. Chen, S. Zhao, M.Y. Chen, W.T. Zhang, J.L. Mao, Y.C. Zhao, M.F. Maitz, N. Huang, G.J. Wan, Sandwiched polydopamine (PDA) layer for titanium dioxide (TiO2) coating on magnesium to enhance corrosion protection, Corrosion Sci. 96 (2015) 67–73.

[50] M. Alishahi, F. Mahboubi, S.M. Mousavi Khoie, M. Aparicio, E. Lopez-Elvira, J. Méndez, R. Gago, Structural properties and corrosion resistance of tantalum nitride coatings produced by reactive DC magnetron sputtering, RSC Adv. 6 (92) (2016) 89061–89072.
[51] C.Y. Li, C. Yu, R.C. Zeng, B.C. Zhang, L.Y. Cui, J. Wan, Y. Xia, In vitro corrosion resistance of a Ta2O5 nanofilm on MAO coated magnesium alloy AZ31 by atomic layer deposition, Bioact. Mater. 5 (1) (2020) 34–43.
[52] A.M. Galow, A. Rebl, D. Koczan, S.M. Bonk, W. Baumann, J. Gimsa, Increased osteoblast viability at alkaline pH in vitro provides a new perspective on bone regeneration, Biochem. Biophys. Rep. 10 (2017) 17–25.
[53] K.K. Kaysinger, W.K. Ramp, Extracellular pH modulates the activity of cultured human osteoblasts, J. Cell. Biochem. 68 (1) (1998) 83–89.
[54] S. Kim, K.J. Lee, Y. Seo, Surface modification of poly(ether imide) by low-energy ion-beam irradiation and its effect on the polymer blend interface, Langmuir 18 (16) (2002) 6185–6192.
[55] V.K. Balla, S. Banerjee, S. Bose, A. Bandyopadhyay, Direct laser processing of a tantalum coating on titanium for bone replacement structures, Acta Biomater. 6 (6) (2010) 2329–2334.
[56] P.K. Mattila, P. Lappalainen, Filopodia: molecular architecture and cellular functions, Nat. Rev. Mol. Cell Biol. 9 (6) (2008) 446–454.
[57] B.S. Moon, S. Kim, H.E. Kim, T.S. Jang, Hierarchical micro-nano structured Ti6Al4V surface topography via two-step etching process for enhanced hydrophilicity and osteoblastic responses, Mater. Sci. Eng. C Mater. Biol. Appl. 73 (2017) 90–98.
[58] U. Meyer, A. Büchter, H.P. Wiesmann, U. Joos, D.B. Jones, Basic reactions of osteoblasts on structured material surfaces, Eur. Cell. Mater. 9 (2005) 39–49.
[59] L. Cai, J. Zhang, J. Qian, Q. Li, H. Li, Y. Yan, S. Wei, J. Wei, J. Su, The effects of surface bioactivity and sustained-release of genistein from a mesoporous magnesium-calcium-silicate/PK composite stimulating cell responses in vitro, and promoting osteogenesis and enhancing osseointegration in vivo, Biomater. Sci. 6 (4) (2018) 842–853.
[60] X.J. He, X.Y. Zhang, J.F. Li, R.Q. Hang, X.B. Huang, X.H. Yao, L. Qin, B. Tang, Titanium-based implant comprising a porous microstructure assembled with nanoleaves and controllable silicon-ion release for enhanced osseointegration, J. Mater. Chem. B 6 (31) (2018) 5100–5114.